## Research Article

Anna Mikhailovskaya, Diana Shakirova*, Sergey Krasikov, Ildar Yusupov, Dmitry Dobrykh,
Alexey Slobozhanyuk, Andrey Bogdanov, Dmitry Filonov and Pavel Ginzburg

# Anapole-enabled RFID security against far-field attacks

**Abstract:** Radio frequency identification (RFID) is a widely used wireless technology for contactless data exchange. Owing to international standardization and one-way security nature of the communication protocol, RFID tags, holding sensitive information, may be a subject to theft. One of the major security loopholes is the so-called far-field attack, where unauthorized interrogation is performed from a distance, bypassing the user's verification. This loophole is a penalty of using a dipole-like RFID tag antenna, leaking wireless information to the far-field. Here we introduce a new concept of anapole-enabled security, prohibiting far-field attacks by utilizing fundamental laws of physics. Our design is based on radiationless electromagnetic states (anapoles), which have high near-field concentration and theoretically nulling far-field scattering. The first property enables performing data readout from several centimeters (near-field), while the second prevents attacks from a distance, regardless an eavesdropper's radiated power and antenna gain. Our realization is based on a compact 3 cm high-index ceramic core–shell structure, functionalized with a thin metal wire and an integrated circuit to control the tag. Switching scheme was designed to provide a modulation between two radiationless anapole states, blocking both up and down links for a far-field access. The anapole tag demonstrates more than 20 dB suppression of far-field interrogation distance in respect with a standard commercial tag, while keeping the near-field performance at the same level. The proposed concept might significantly enhance the RFID communication channel in cases, where information security prevails over cost constrains.

**Keywords:** anapole; multipole engineering; RFID technology; scattering.

## 1 Introduction

Radio frequency identification (RFID) is one of the commonly used approaches to a short-range wireless data exchange. In passive RFID architectures, the data is encoded on a passive device, consisting of an integrated circuit (IC) and an antenna. Active reader interrogates the tag and receives information encoded on the time-modulated backscattered signal. This realization puts the main complexity and the cost on the reader's size, keeping the tag on a consumable level. Significant efforts have been applied to develop different tag's antenna architectures. Those include meander antennas [1], fractal dipole [2]. It is worth noting that tag's antennas are designed per application, where an environment plays a significant role. For example, labeling textile or metal-containing goods put different demands on RF design [3, 4].

It is also worth mentioning other antenna designs, which were developed for different applications, including 5G technologies [5–8] wireless communication devices [9–16], and radars [17].

Being a widespread wireless technology, RFID is a subject to international regulations and standardizations, coming with their pros and cons. Being very convenient, the capability to readout data from any tag by any reader, obeying the same standard, opens a big security loophole of unauthorized access. Apart from simple logistic warehouses applications, RFID tags are used to hold sensitive

*Corresponding author: Diana Shakirova, School of Physics and Engineering, ITMO University, Saint-Peterburg, 197101, Russia, E-mail: diana.shakirova@metalab.ifmo.ru. https://orcid.org/0000-0003-4560-0117
Anna Mikhailovskaya, Dmitry Dobrykh and Pavel Ginzburg, School of Electrical Engineering, Tel Aviv University, Tel Aviv 69978, Israel
Sergey Krasikov, Ildar Yusupov, Alexey Slobozhanyuk and Andrey Bogdanov, School of Physics and Engineering, ITMO University, Saint-Peterburg 197101, Russia. https://orcid.org/0000-0003-3773-2988 (S. Krasikov). https://orcid.org/0000-0002-8215-0445 (A. Bogdanov)
Dmitry Filonov, Center for Photonics and 2D Materials, Moscow Institute of Physics and Technology, Dolgoprudny 141700, Russia. https://orcid.org/0000-0002-5394-8677

information, related to e.g. biometric passports, credit cards, entrance permits, and many others. A typical credit card theft is performed by approaching a victim with a reader. Small transactions do not require an authorization, opening a significant security loophole, which is a penalty of using wireless technologies for customers' convenience. However, those types of attacks are performed from short distances owing to aspects of low frequency (125 KHz, 13.56 MHz) electromagnetic designs. Hereinafter, this loophole will be called a near-field attack.

Ultrahigh frequency (UHF) RFID systems operate in the 860–960 MHz bands (EPCGEN2 standard), making free-space propagation mechanisms to control the physics of the communication channel. While typical commercially available UHF RFID systems are designed to perform at centimeter-level distances, custom modifications can enlarge the operation range towards 10–20 m and even more. This is done by introducing a directive antenna on the reader's side – the interrogation range grows proportionally to the square root of the gain in a linear scale [18–20]. The reading distance can be further increased by introducing amplifiers. While international regulations limit effective isotropic radiated power (EIRP) to 2–4 W, depending on a licensing country, those bounds are obviously cannot be taken as granted in the case of theft attempts. As a result, extremely long-range unauthorized data readout can be performed, underlining a big security loophole in RFID technology. Since the attack, in this case, is performed from a range, prevailing free space operational wavelength, hereinafter it will be called a *far-field attack*.

The goal of our investigation is to develop a tag, which will be immune to far-field attacks and, on the other hand, will be freely accessible from a short distance, maintaining the wireless nature of the RFID communication channel. The security in this case is not provided by a software encryption, but granted by antenna design, ensuring unconditional operation in the frame of the RFID standard. From the electromagnetic standpoint, this principle can be realized if a considerable near-field accumulation is accompanied with a vanishing antenna far-field. The first property is responsible for reliable wireless data readout from a short range, while the second one fundamentally blocks accessibility from a distance. In this context it is worth mentioning other approaches to address this issue. Those include subwavelength tag's antennas with poor radiation efficiency and degraded on purpose and RFID chips with elevated activation threshold [21, 22]. Those solutions lead to ~30 dB reading distance drop, if

conventional EIRPs are used. While those realizations grant a high level of security against conventional readers, they cannot ensure it on the most fundamental level, at least theoretically. As the result, new approaches for hardware security might be of a value. RFID security, being an important issue, can be also addressed with other approaches [23, 24].

Investigation of radiationless distributions of electromagnetic currents takes the route back to the early stages of quantum mechanics, where electron collapse on a nucleus in the frame of Bohr's model was attempted to be explained. In particular, a family of nontrivial current trajectories, generated by moving charged carriers in space, was found [2]. While this theory lost its relevance with the development of the Schrodinger equation and probabilistic postulates of the quantum nature, it gave rise to new investigations in the field of nanophotonics. One of the most remarkable examples of the nonradiating current configuration is *anapole*. Being introduced by Zeldovich in 1957 [25], anapole formalism has got a new twist in all-dielectric nanophotonics. Observations of those states are possible in various geometries, including spherical particles, comprehensively described by Mie theory [26–28]. Anapoles were also taken towards practical applications, including compact lasers [29], nanoantenna's with enhanced second and third harmonic generation [30–33], nonradiating energy transfer [34, 35], and magnetic dipole sources [36]. Anapoles were utilized to enhance Raman scattering [37] and light absorption in photonic nanostructures, including nanodisks and core–shell particles [38–40]. Evolving applications also include anapole-driven metamaterials [41–43] and anapole interactions with molecular excitations [44]. Anapoles were also found in bio-inspired structures [45–47].

Here we propose to utilize anapole states for hardware protection of RFID tags against far-field attacks. While the general concept of radiationless currents grants the far-field suppression by design, RFID operation is quite different from a simple plane wave scattering. On a high level, the communication channel can be split into two parts. Downlink is the weak up of the tag, illuminated by the reader. High frequency electromagnetic currents, excited on the tag's antenna, are rectified by the IC and power the modulator, which switches antenna impedance to transmit a 96-bit number stored in the chip's memory. Backpropagation of the time-modulated reflection and signal's reception by reader's antenna is the uplink of the communication channel. In order to provide robust hardware security against far-field attacks, switching between

two impedance states of the IC should maintain the overall structure at the anapole state. In other words, a structure, supporting electronically switchable anapole states, should be designed to comply with RFID architecture. Here we design a new structure, based on a high index ceramic core–shell, functionalized with a short metal wire and a modulation circuit. Switching the impedance of the modulation circuit modulates the system at an anapole state, virtually blocking both up and downlinks.

The manuscript is organized as follows – the concept of switchable anapole states is presented and analyzed in frame of Mie theory, which allows performing fast semi-analytical optimization of spherical core–shell geometries. An IC is introduced next and optimized to provide switching capabilities. RFID operation and far-field attach suppression is analyzed before conclusion.

## 2 Optimization of core–shell geometry

### 2.1 Optimization with Mie theory

High-index dielectric resonators support a variety of electromagnetic modes, which are governed by structure's geometry and a real part of the refractive index of constitutive materials. Adjustment of those parameters allows designing combinations of several interfering multipoles, e.g. [48, 49]. Furthermore, mixing high-quality ceramics powders enables considering refractive index as an additional engineering parameter, ranging from moderately low to extremely high values, approaching hundreds [50]. The later property allows achieving significant size reduction of a resonator.

Electromagnetic properties of structures with spherical symmetries can be assessed semi-analytically with the aid of Mie theory, which is beneficial for performing computationally efficient parametric studies over a large search space. A core–shell geometry was chosen as a starting point for optimization with the goal of obtaining a pair of anapole states. Those should be located close to each other in a parametric map. In this case an efficient modulation scheme to switch between them can be made possible. Once two anapole states, corresponding to zeroing of the scattering efficiency are obtained, a control element, capable of switching between those two, will be developed. This switching is essential for the RFID operation.

The initial structure, which consists of a concentric sphere, shell (with a different refractive index), and an air interlayer between them, has five degrees of freedom (radiuses and refractive indices of the materials). Those are sufficient for controlling the hierarchy of resonant multipoles. Scattering efficiency is given by [51]:

$$Q_{sca} = \frac{2}{(kr)^2} \sum_{n=1}^{\infty} (2n+1)\left(|a_n|^2 + |b_n|^2\right), \qquad (1)$$

where $k$ is a wavenumber outside the structure, $r$ is outer radius of the shell, and $a_n$ and $b_n$ are Mie coefficients associated with electric and magnetic multipoles, respectively. In this case, spherical harmonics are taken as the expansion basis. Mutual orthogonality of the basis functions allows associating each spherical harmonic with an independent scattering channel. In particular, complex-plane poles of the scattering Mie coefficients correspond to the eigenmodes of the resonator. Nulls of the coefficients, lying on the real axis, correspond to anapoles – zero energy flow into a single scattering channel or, in other words, a vanishing partial cross-section. This definition will be used hereinafter. Hence, the anapole is not an eigenstate of a system, as it corresponds to the null but not to the pole of the scattering coefficient. Furthermore, anapole's existence can be considered only in conjugation with the incident field.

While the anapole state is an effect of vanishing scattering into a single scattering channel, it is frequently associated with an emergence of toroidal moments, destructively interfering with other multipoles [52–55]. However, as it was recently shown, the toroidal moments are not additional missing basis functions in the multipolar expansion, but they appear as higher-order corrections to approximate expressions for multipole moments, derived within to long-wavelength limit [29, 30].

To find the anapole state in our spherical core–shell geometry, a color map presenting $Q_{sca}$ as a function of core refractive index and operational frequency is plotted in Figure 1. The upper bound on the size of the structure was chosen to be 3 cm to keep the tag's footprint reasonable. The radius of the core is chosen to be 8 mm, the thicknesses of the intermediate air layer and shell are 1.5 mm and 5.5 mm, respectively. In practice, air gap can be filled with any RF-transparent material, e.g. polystyrene. After a set of preliminary assessments and considerations of experimentally available refractive indexes, the shell parameter was fixed to $n_{shell} = 29$. The core index was varied in the range $n_{core} = 26$–$32$. The imaginary part of refractive index was taken to be $\kappa = 0.01$, which complies with experimental data [50]. The relevant regions are highlighted with a black (first anapole state) and red (second anapole state) dashed circle. Two anapole states were found within the RFID frequency band (954–956 MHz) at $n_{core} = 27.5$ and $n_{core} = 31$, which will correspond to state 1 and state 2 of a modulation
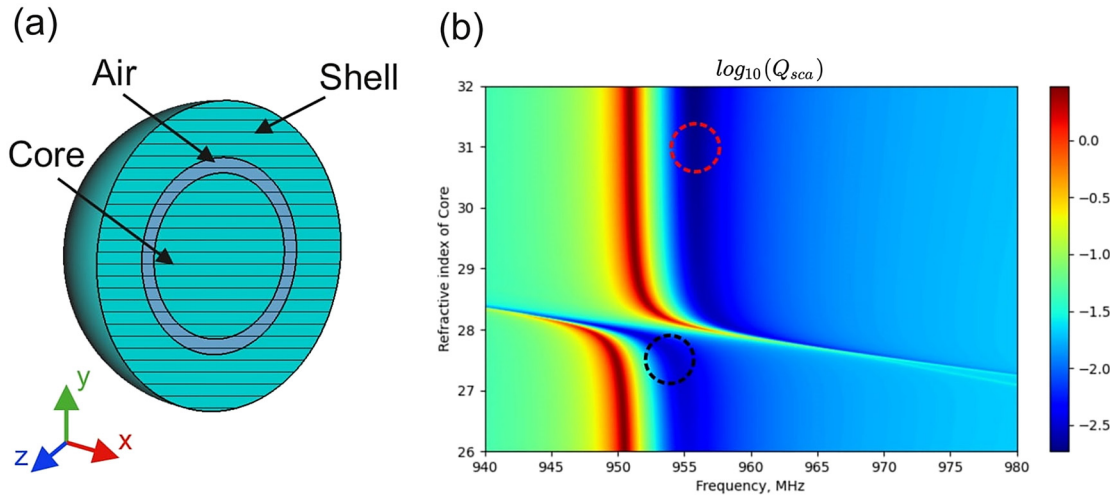
**Figure 1:** Scattering efficiency of the model.
(a) Core–shell geometry (b) color map (logarithmic scale) of scattering efficiency as a function of the cores' refractive index and the operational frequency. The inner sphere's radius is 8 mm, and thickness of the air interlayer and shell are 1.5 mm and 5.5 mm, respectively. Shell's refractive index is $n_{shell} = 29$.

scheme (Figure 1). One of the design aims is to reduce the footprint of the tag, elevating the refractive indices (permittivity up to 1000 is possible, based on available ceramic powders) of constitutive components. An excessive size reduction, on the other hand, leads to the bandwidth degradation. In this case, at least a single the RFID communication channel should be supported.

It is worth noting that modulating the refractive index is not practical, nevertheless it allows capturing the main physical principle and provides guidelines for further numerical optimization with an IC. This will be done hereafter.

## 2.2 Multipole engineering of modulation

Design of the core–shell structure, supporting two regimes of vanishing scattering cross-sections in the RFID frequency range (EPC Gen2, 860–960 MHz), was demonstrated in the previous section. This phenomenon was attributed to the emergence of anapole states, which will be proven now. For this purpose we provide a multipole expansion of the scattering cross-section (SCS) in Cartesian coordinates, using the analytical expression [56]:

$$C_{sca} \approx \frac{k^4}{6\pi\epsilon_0^2|E_0|^2}\left[\sum_\alpha\left(|p_\alpha|^2 + \left|\frac{m_\alpha}{c}\right|^2\right) + \frac{1}{120}\sum_{\alpha\beta}\left(|kQ_{\alpha\beta}^e|^2 + \left|\frac{kQ_{\alpha\beta}^m}{c}\right|^2\right)\right], \quad (2)$$

where $E_0$ is the amplitude of the incident plane wave, $\epsilon_0$ is the vacuum permittivity, and $c$ is the speed of light in the free space. Indices $\alpha, \beta$ run over the Cartesian coordinates $x, y, z$.

Electric and magnetic dipole moments $p_\alpha$ and $m_\alpha$, as well as electric and magnetic quadrupole moments $Q_{\alpha\beta}^e$ and $Q_{\alpha\beta}^m$ are obtained with exact expressions introduced in Ref. [57]:

$$p_\alpha = \frac{-1}{i\omega}\left\{\int d^3r J_\alpha j_0\,(kr) + \frac{k^2}{2}\int d^3r[3\,(r\cdot J)r_\alpha - r^2 J_\alpha]\frac{j_2\,(kr)}{(kr)^2}\right\}, \quad (3)$$

$$m_\alpha = \frac{3}{2}\int d^3r\,(r\times J)_\alpha\frac{j_1\,(kr)}{kr}, \quad (4)$$

$$Q_{\alpha\beta}^m = 15\int d^3r\{r_\alpha\,(r\times J)_\beta + r_\beta\,(r\times J)_\alpha\}\frac{j_2\,(kr)}{(kr)^2}, \quad (5)$$

$$Q_{\alpha\beta}^e = \frac{-3}{i\omega}\left\{\int d^3r[3\,(r_\beta J_\alpha + r_\alpha J_\beta) - 2\,(r\cdot J)\delta_{\alpha\beta}]\frac{j_1\,(kr)}{kr}\right.$$
$$+ 2k^2\int d^3r[5r_\alpha r_\beta\,(r\cdot J) - (r_\alpha J_\beta + r_\beta J_\alpha)r^2 \quad (6)$$
$$\left. - r^2\,(r\cdot J)\delta_{\alpha\beta}]\frac{j_3\,(kr)}{(kr)^3}\right\},$$

where $\omega$ is a frequency, $J$ is the induced electric current density, $r$ is the radius vector and $j_n$ ($n = 0, 1, 2, 3$) are the spherical Bessel functions. Note, that Eq. (1) uses spherical harmonics basis, while Eq. (2) makes the expansion in Cartesian system. However physical meaning of multipole moments is independent from their basis as for any physical quantity. Calculation of the moments is done with COMSOL Multiphysics®. In particular, we solve scattering problem numerically, obtain the current density and then substitute it to Eqs. (3)–(6).

The corresponding spectra of the SCSs in the range of 948–958 MHz are shown in Figure 2. The geometry is taken
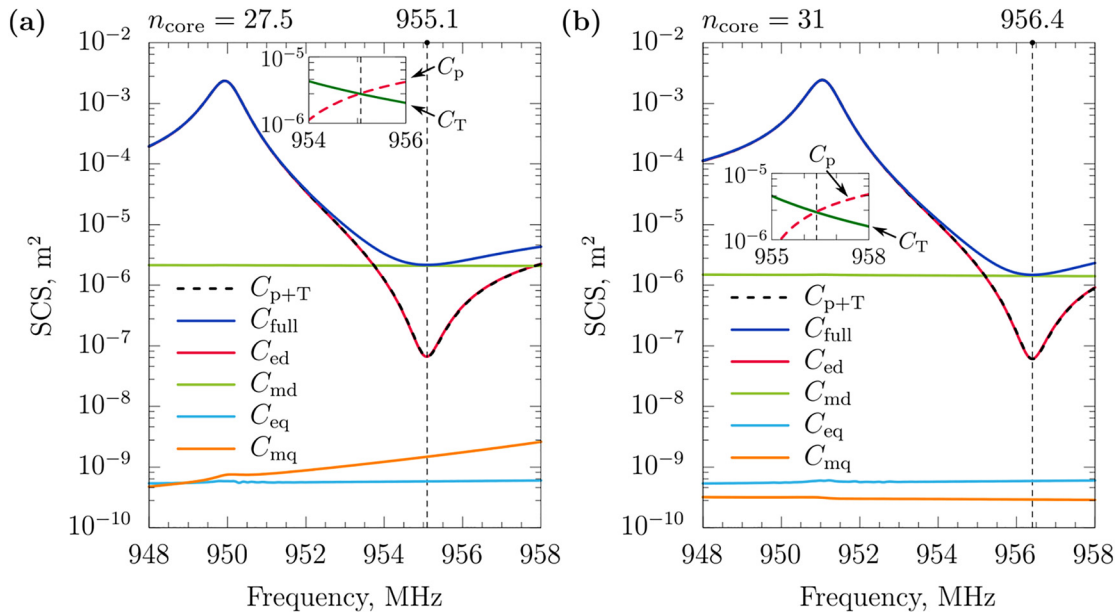
**Figure 2:** Multipole expansion of the scattering cross-section (SCS is in logarithmic scale) of the core–shell particle with the refractive index of the core (a) $n_{core} = 27.5$ and (b) $n_{core} = 31$. The expansion is done up to the quadrupole order, such that $C_{full}$ is the sum of the calculated partial cross-sections. $C_{p+T}$ is the contribution of the toroidal dipole moment and the electric dipole moment in the long-wavelength approximation. Black dashed curve $C_{p+T}$ overlaps with the red curve, corresponding to the partial SCS of fully-retarded electric dipole moment $C_{ed}$. Insets demonstrate $C_p$ and $C_T$ corresponding to contributions of $p^{app}$ and $T$, respectively. Vertical black dashed lines correspond to the SCS minima at (a) 955.1 MHz and (b) 956.4 MHz.

from the previous section. The total SCS is governed by the non-resonant residual magnetic dipole, while electric dipole scattering channel vanishes if two special frequencies are considered – 955.1 MHz for $n_{core} = 27.5$ [Figure 2(a)] and 956.4 MHz for $n_{core} = 31$ [Figure 2(b)]. These dips in the spectra are the anapole states, which were identified by observing Figure 1(b). Those specific frequencies can be further tuned by varying the geometry and swept over the entire RFID frequency band. In addition, here we will demonstrate that toroidal moments are only quasi-static corrections in the frame of the long-wavelength approximation, and can be avoided by using the exact expressions. For this purpose, partial SCS is calculated as a coherent sum of the approximated electric dipole moment $p_\alpha^{app}$ and toroidal dipole moment $T_\alpha$, obtained via the conventional expressions [55]:

$$C_{p+T} = \frac{k^4}{6\pi\epsilon_0^2|E_0|^2}\sum_\alpha\left|p_\alpha^{app} + \frac{ik}{c}T_\alpha\right|^2, \qquad (7)$$

$$p_\alpha^{app} = \frac{-1}{i\omega}\int d^3r J_\alpha, \quad T_\alpha = \frac{1}{10}\int d^3r\left[(r\cdot J)r_\alpha - 2r^2 J_\alpha\right]. \qquad (8)$$

The results of the calculations are also shown in Figure 2 by dashed black lines. As it was expected, $C_{p+T}$ and $C_{ed}$ completely overlaps indicating that the toroidal dipole moment is needed only to correct an approximated value of

the electric dipole moment. Here, $p_\alpha^{app}$ is calculated via Taylor expansion of currents in the source region [58], while Eq. (3) for $p_\alpha$ is an exact expression obtained without any approximations. In addition, insets in Figure 2 demonstrate values of $C_p$ and $C_T$, which are partial SCSs calculated via Eq. (4) for $p^{app}$ and $T$, respectively. Each of them do not vanish in the region of interest; however their interference results in a dip, reducing the partial CSC by two orders of magnitude.

# 3 Switching between anapole states with an integrated circuit

## 3.1 Design of the structure

While the theoretical model with fast Mie theory-based optimization allows assessing a range of relevant parameters, an outlook to a practical implementation suggests employing an IC for the switching. In this case, closed-form Mie solutions do not exist. Hereinafter, we will consider a short dipole with a switch, plugged in a gap [Figure 3(a)].

A full-wave numerical simulation in CST MICROWAVE STUDIO, frequency-domain solver, was used for designing the structure. We optimize the switching between two
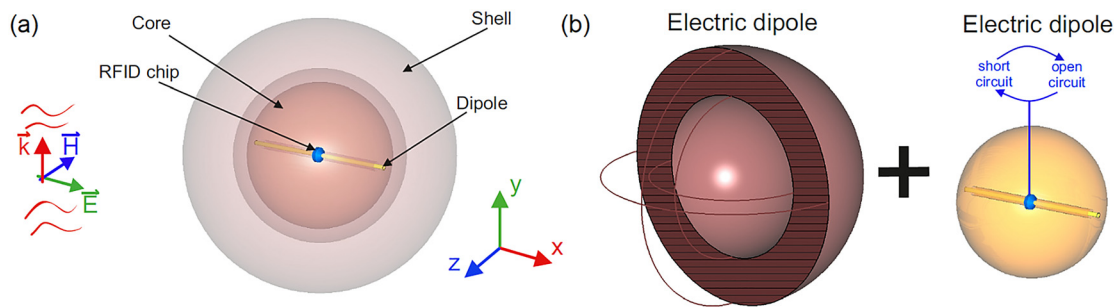
**Figure 3:** Schematics of an RFID tag.
(a) A core–shell ceramic structure and dipole with an RFID chip, soldered within a gap. (b) The principle of operation – destructive interference between electric dipolar resonances in the shell and in the core. The impedance, soldered within a gap of a thin wire, controls the dipolar resonance of the core, switching between two anapole states of the structure.

anapole of the core–shell, which was analyzed in the previous section. In the theoretical model, we vary the core's refractive index to null the scattering into dipolar channel. However, this approach cannot be implemented in practice. To shift ED resonance of the core with an IC, we introduce a metal wire, passing through the center of the structure (Figure 3). This strategy was chosen since the ED of the core has a maximum electric field at the center and as the result, might have a sufficient coupling with the ED of the metal wire. Thus, modulating the impedance of the wire (open and short circuit in the middle gap), we change its coupling with the core and control the resonance of the latter.

The design, shown in Figure 3(a), consists of a shell tuned to ED (see Figure 3(b)) and a core, functionalized with a small dipole + IC (see Figure 3(b)). The previously discussed geometry was used as an initial starting point for the optimization. Changes, introduced by inserting the wire within the shell were compensated by varying parameters around their initial values. After a set of optimizations, the parameters are: the core's radius $r_{core} = 8$ mm

and inner and outer radiuses of the shell $r_{inner\ shell} = 9.5$ mm and $r_{outer\ shell} = 15$ mm (there is a 1.5-mm-wide air layer between the core and the shell). The real and imaginary part of refractive indices of shell and core was taken from the theoretical model. A cylindrical hole with a radius of 0.5 mm was made through the core to host the copper wire (electric conductivity $\sigma = 5.8 \times 10^7$ S/m). Plane wave excited the structure in a way that the electric field vector was directed along copper wire.

Commercial RFID ICs typically have complex impedances in modulation states and may vary from vendor to vendor. Here we will use a pair of our custom-designed impedances to control the structure. Metal wire shifts the resonances of the initial structure to higher frequencies. To compensate for the shift, we added a lumped coil with $L = 47$ nH. This state will correspond to State 2. State 1 corresponds to $L = 111$ nH. Thus, modulating the impedance of the dipole (inductance) we switch between two anapole states (see Figure 4). As it was mentioned previously, the structure in State 1 has two nearby anapoles. IC shifts the higher frequency state to the spectral location of
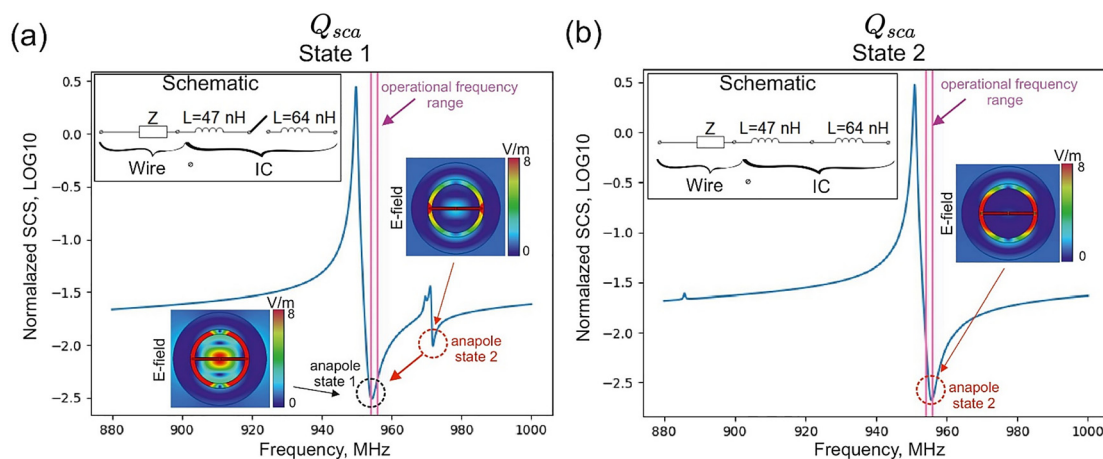


**Figure 4:** Scattering efficiencies of the structure for (a) "state 1" – $L = 111$ nH and (b) "state 2" – $L = 47$ nH. Inserts – absolute values of electrical field amplitude in anapole states.

the first one. As the result, the tag remains in the anapole state for both of the impedance nominals, ensuring the far-field leakage suppression. The inserts in Figure 4 show absolute values of electric field amplitudes in two anapole states and verify that the high-frequency anapole was shifted from 972 MHz to 955 MHz by changing the IC inductance.

## 3.2 Tag's security assessment

To verify the proposed hardware security scheme, our design will be assessed versus a standard commercial realization and a pair of special short-range tags. Both near- and far-field readout performances will be estimated. Six-element linearly polarized Yagi-Uda was designed to operate at 900–990 MHz and was used to interrogate the tags [Figure 5(a)]. Antenna's gain is 11.5 dBi. Near-field distance was chosen to be 3 cm, while far-field scenario is 1 m. Complex reflection coefficients ($S_{11}$ parameters) were calculated. Modulation efficiency (absolute value of a difference between $S_{11}$ parameters of two states ($|S^{(1)}_{11}-S^{(2)}_{11}|$)) plays a significant role in tag's operation. Our anapole tag can be further optimized by considering this criterion – the modulation efficiency should be maximized at the near-field and suppressed at the far-field. For this purpose, we kept $L = 47$ nH (State 2) constant, while varying the inductance at State 1 from 60 nH to 120 nH. Figure 5(b) shows the near- and far-field modulation efficiencies as the function of the inductance. It can be seen that nearly

maximal contrast at the near-field and the dip for the far-field case is obtained for $L = 111$ nH, exactly as it was designed to support the switchable anapole state. While the anapole design was made for a plane wave incidence, considering a practical interrogating antenna might introduce variations. Figure 5(b) shows the modulation efficiency as a function of frequency. Here, $L = 111$ nH in State 1 was kept constant. A minor shift of the operational frequency can be observed. Under those optimal conditions, 34 dB difference in the modulation efficiency at near- and far-fields can be observed.

In order to assess the far-field security, granted by the anapole design, commercial ALN-9654-FWRW tag and near-field tags (GEE-UT-J41 Impinj J41 UHF tag, J51 Impinj Monza5 tag) were used for a reference. Table 1 summarizes the results and shows a minor advantage of the anapole tag in near-field interrogation along with more than an order two of magnitude suppression of the far-field leakage compared to the standard dipole tag and an order of magnitude compared to the short-range desighns. In other words, the anapole tag grants an ordinary short-range operation, while the far-field attack is significantly suppressed. To attack the anapole tag with the same success, as it is possible with a commercial tag, 100 times increase of the reader's radiated power is needed. Introducing an IC with a low activation threshold, as it is done in GEE-UT-J41 Impinj J41 and J51 Impinj Monza5 tags [59], can improve the security furthermore. Our tag can be further improved by suppressing the residual magnetic dipole moment, as it can be seen from Figure 2.
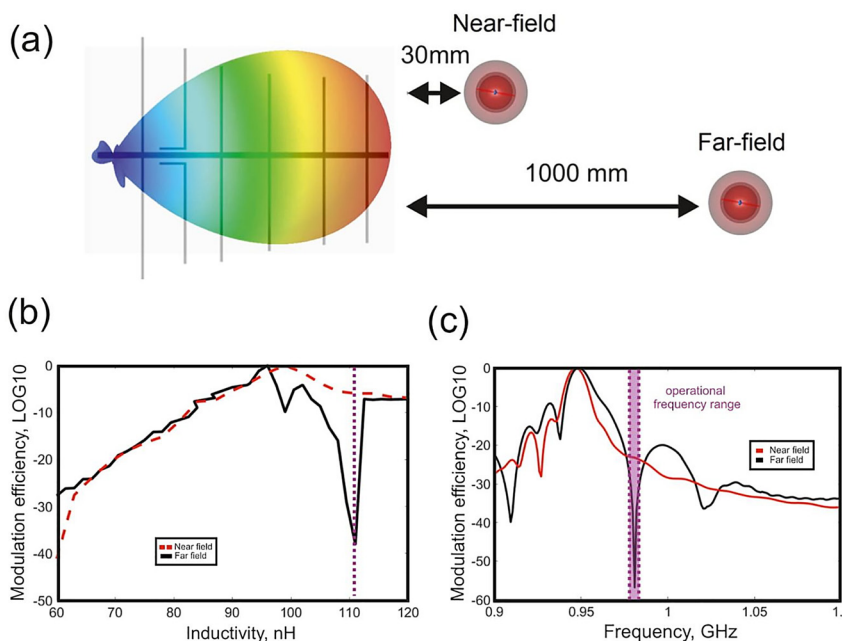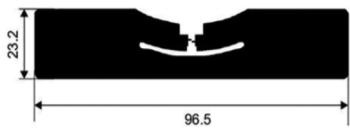


**Figure 5:** Tag's security assessment in near- and far- fields.
(a) Near- and far-field interrogation schemes. (b) Near- and far-field modulation efficiencies, as the function of the lumped element induction in state 1. (c) Near- and far-field modulation efficiencies, as the function of the operation frequency. $L = 111$ nH in state 1 is kept constant.

**Table 1:** Modulation depth $|S^{(1)}_{11} - S^{(2)}_{11}|$, comparison between different tags.

| | Anapole RFID tag | ALN-9654-FWRW tag | GEE-UT-J41 Impinj J41 | J51 Impinj Monza5 tag |
|---|---|---|---|---|
| Near-field (0.03 m) | $5 \times 10^{-3}$ | $2.5 \times 10^{-3}$ | $2.2 \times 10^{-4}$ | $2.5 \times 10^{-4}$ |
| Far field (1 m) | $5.5 \times 10^{-6}$ | $4 \times 10^{-4}$ | $1.8 \times 10^{-5}$ | $2.2 \times 10^{-5}$ |

# 4 Conclusions

Hardware protection of RFID tags against far-field attacks was proposed and assessed from the electromagnetic standpoint. Radiotionless anapole states were introduced within tag's antenna design and granted significant near-field accumulation with almost complete suppression of far-field signatures. A switchable impedance of the integrated circuit was designed to modulate the system between two anapoles, preventing information leakage regardless the tag's state and making the information holder invisible to a far-field interrogation. The proposed design is 3 cm in diameter, making this volumetric footprint suitable for UHF RFID applications. The demonstrated anapole protection covers 2 MHz band, which complies with regulations in the field. While the proposed design may face challenges in practical realizations, it can be replicated to other geometrical arrangements, complying with planar architectures, which are more appropriate from a practical standpoint.

RFID anapole protection, granted by fundamental laws of nature, can find a use in a range of sensitive applications, where information security is essential from both technological and psychological standpoints. It is worth emphasizing other existent solutions, including antenna efficiency and IC sensitivity degradation. Those approaches benefit from existing RFID planar architectures and comply with footprint and cost requirements. Being attractive from the practical standpoint, those solutions can fail against aggressive far-field attacks, where EIRP is not limited by international regulations. Anapole protection, on the other hand, can grant the fundamental level of security, at least on the theoretical level. If this aspect prevails over other practical constrains, a new generation of tags can be a legitimate solution.

# References

[1] J. Rashed and C. T. Tai, "Communications a new class of resonant antennas," *IEEE Trans. Antenn. Propag.*, vol. 39, no. 9, pp. 1428–1430, 1991.

[2] H. Kimouche and H. Zemmour, "A compact fractal dipole antenna for 915 MHz and 2.4 GHz RFID tag applications," *Prog. Electromagn. Res. Lett.*, vol. 26, pp. 105–114, 2011.

[3] A. A. Babar, T. Bjorninen, V. A. Bhagavati, L. Sydanheimo, P. Kallio, and L. Ukkonen, "Small and flexible metal mountable passive UHF RFID tag on high-dielectric polymer-ceramic composite substrate," *IEEE Antenn. Wireless Propag. Lett.*, vol. 11, pp. 1319–1322, 2012.

[4] M. Alibakhshi-Kenari, M. Naser-Moghadasi, R. Ali Sadeghzadeh, B. S. Virdee, and E. Limiti, "Dual-band RFID tag antenna based on the Hilbert-curve fractal for HF and UHF applications," *IET Circ. Dev. Syst.*, vol. 10, no. 2, pp. 140–146, 2016.

[5] M. Alibakhshikenari, F. Babaeian, B. S. Virdee, et al., "A comprehensive survey on 'various decoupling mechanisms with focus on metamaterial and metasurface principles applicable to SAR and MIMO antenna systems," *IEEE Access*, vol. 8, pp. 192965–193004, 2020.

[6] N. Ojaroudi Parchin, H. Jahanbakhsh Basherlou, M. Alibakhshikenari, et al., "Mobile-phone antenna array with diamond-ring slot elements for 5G massive MIMO systems," *Electronics*, vol. 8, no. 5, p. 521, 2019.

[7] M. Alibakhshikenari, B. S. Virdee, P. Shukla, et al., "Isolation enhancement of densely packed array antennas with periodic MTM-photonic bandgap for SAR and MIMO systems," *IET Microw. Antennas Propag.*, vol. 14, no. 3, pp. 183–188, 2020.

[8] M. Alibakhshi-Kenari, M. Movahhedi, and H. Naderian, "A new miniature ultra-wide band planar microstrip antenna based on the metamaterial transmission line," in 2012 IEEE Asia-Pacific Conference on Applied Electromagnetics (APACE), 2012, pp. 293–297.

[9] M. Alibakhshi-Kenari, M. Naser-Moghadasi, R. A. Sadeghzadeh, B. S. Virdee, and E. Limiti, "A new planar broadband antenna based on meandered line loops for portable wireless communication devices," *Radio Sci.*, vol. 51, no. 7, pp. 1109–1117, 2016.

[10] M. Alibakhshikenari, E. Limiti, M. Naser-Moghadasi, B. S. Virdee, and R. A. Sadeghzadeh, "A new wideband planar antenna with band-notch functionality at GPS, Bluetooth and WiFi bands for integration in portable wireless systems," *AEU Int. J. Electron. Commun.*, vol. 72, pp. 79–85, 2017.

[11] R. A. Sadeghzadeh, M. Alibakhshi-Kenari, and M. Naser-Moghadasi, "UWB antenna based on SCRLH-TLs for portable wireless devices," *Microw. Opt. Technol. Lett.*, vol. 58, no. 1, pp. 69–71, 2016.

[12] M. Alibakhshikenari, B. S. Virdee, L. Azpilicueta, et al., "A comprehensive survey of 'metamaterial transmission-line based antennas: design, challenges, and applications," *IEEE Access*, vol. 8, pp. 144778–144808, 2020.

[13] M. Alibakhshikenari, B. S. Virdee, C. H. See, R. A. Abd-Alhameed, F. Falcone, and E. Limiti, "High-gain metasurface in polyimide on-chip antenna based on CRLH-TL for sub-terahertz integrated circuits," *Sci. Rep.*, vol. 10, no. 1, p. 4298, 2020.

[14] M. Alibakhshi-Kenari, M. Naser-Moghadasi, and R. Sadeghzadeh, "The resonating MTM-based miniaturized antennas for wide-band RF-microwave systems," *Microw. Opt. Technol. Lett.*, vol. 57, no. 10, pp. 2339–2344, 2015.

[15] M. Alibakhshi-Kenari, M. Naser-Moghadasi, R. Ali Sadeghzadeh, and B. Singh Virdee, "Metamaterial-based antennas for integration in UWB transceivers and portable microwave handsets," *Int. J. RF Microw. Comput. Eng.*, vol. 26, no. 1, pp. 88–96, 2016.

[16] M. A. Kenari, "Printed planar patch antennas based on metamaterial," *Int. J. Electron. Lett.*, vol. 2, no. 1, pp. 37–42, 2014.

[17] M. Alibakhshikenari, B. S. Virdee, and E. Limiti, "Wideband planar array antenna based on SCRLH-TL for airborne synthetic aperture radar application," *J. Electromagn. Waves Appl.*, vol. 32, no. 12, pp. 1586–1599, 2018.

[18] F. K. Byondi and Y. Chung, "Longest-range UHF RFID sensor tag antenna for IoT applied for metal and non-metal objects," *Sensors*, vol. 19, no. 24, p. 5460, 2019.

[19] A. Choudhary, D. Sood, and C. C. Tripathi, "Wideband long range, radiation efficient compact UHF RFID tag," *IEEE Antenn. Wireless Propag. Lett.*, vol. 17, no. 10, pp. 1755–1759, 2018.

[20] D. Dobrykh, I. Yusupov, S. Krasikov, et al., "Long-range miniaturized ceramic RFID tags," *IEEE Trans. Antenn. Propag.*, vol. 69, no. 6, pp. 3125–3131, 2021.

[21] Z. Xing, "Near-field antenna of RFID system," in *Radio Frequency Identification*, InTech, 2017, https://doi.org/10.5772/intechopen.71427.

[22] D. Liu, R. Wang, K. Yao, X. Zou, and L. Guo, "Design and implementation of a RF powering circuit for RFID tags or other batteryless embedded devices," *Sensors*, vol. 14, no. 8, pp. 14839–14857, 2014.

[23] B.-Q. Zhao, H.-M. Wang, and P. Liu, "Safeguarding RFID wireless communication against proactive eavesdropping," *IEEE Internet Things J.*, vol. 7, no. 12, pp. 11587–11600, 2020.

[24] Q. Yang, H.-M. Wang, Q. Yin, and A. L. Swindlehurst, "Exploiting randomized continuous wave in secure backscatter communications," *IEEE Internet Things J.*, vol. 7, no. 4, pp. 3389–3403, 2020.

[25] Y. B. Zel'dovich, "Electromagnetic interaction with parity violation," *Sov. J. Exp. Theor. Phys.*, vol. 33, p. 1531, 1957.

[26] B. Stout and R. McPhedran, "Egocentric physics: just about Mie," *EPL Europhys. Lett.*, vol. 119, no. 4, p. 44002, 2017.

[27] J. S. Totero Gongora, G. Favraud, and A. Fratalocchi, "Fundamental and high-order anapoles in all-dielectric metamaterials via Fano–Feshbach modes competition," *Nanotechnology*, vol. 28, no. 10, p. 104001, 2017.

[28] I. Fernandez-Corbaton, S. Nanz, R. Alaee, and C. Rockstuhl, "Exact dipolar moments of a localized electric current distribution," *Opt. Express*, vol. 23, no. 26, p. 33044, 2015.

[29] J. S. Totero Gongora, A. E. Miroshnichenko, Y. S. Kivshar, and A. Fratalocchi, "Anapole nanolasers for mode-locking and ultrafast pulse generation," *Nat. Commun.*, vol. 8, no. 1, p. 15535, 2017.

[30] M. Timofeeva, L. Lang, F. Timpu, et al., "Anapoles in free-standing III–V nanodisks enhancing second-harmonic generation," *Nano Lett.*, vol. 18, no. 6, pp. 3695–3702, 2018.

[31] G. Grinblat, Y. Li, M. P. Nielsen, R. F. Oulton, and S. A. Maier, "Enhanced third harmonic generation in single germanium nanodisks excited at the anapole mode," *Nano Lett.*, vol. 16, no. 7, pp. 4635–4640, 2016.

[32] T. Shibanuma, G. Grinblat, P. Albella, and S. A. Maier, "Efficient third harmonic generation from metal–dielectric hybrid nanoantennas," *Nano Lett.*, vol. 17, no. 4, pp. 2647–2651, 2017.

[33] V. F. Gili, L. Ghirardini, D. Rocco, et al., "Metal–dielectric hybrid nanoantennas for efficient frequency conversion at the anapole mode," *Beilstein J. Nanotechnol.*, vol. 9, pp. 2306–2314, 2018.

[34] S.-D. Liu, Z.-X. Wang, W.-J. Wang, J.-D. Chen, and Z.-H. Chen, "High Q-factor with the excitation of anapole modes in dielectric split nanodisk arrays," *Opt. Express*, vol. 25, no. 19, p. 22375, 2017.

[35] J. Tian, H. Luo, Y. Yang, et al., "Active control of anapole states by structuring the phase-change alloy $Ge_2Sb_2Te_5$," *Nat. Commun.*, vol. 10, no. 1, p. 396, 2019.

[36] T. Feng, Y. Xu, W. Zhang, and A. E. Miroshnichenko, "Ideal magnetic dipole scattering," *Phys. Rev. Lett.*, vol. 118, no. 17, p. 173901, 2017.

[37] D. G. Baranov, R. Verre, P. Karpinski, and M. Käll, "Anapole-enhanced intrinsic Raman scattering from silicon nanodisks," *ACS Photonics*, vol. 5, no. 7, pp. 2730–2736, 2018.

[38] R. Wang and L. Dal Negro, "Engineering non-radiative anapole modes for broadband absorption enhancement of light," *Opt. Express*, vol. 24, no. 17, p. 19048, 2016.

[39] J. Wang, N. Wang, J. Hu, and R. Jiang, "Toroidal dipole-induced absorption and scattering dip in (dielectric core)@(plasmonic shell) nanostructures," *Opt. Express*, vol. 25, no. 23, p. 28935, 2017.

[40] E. Zanganeh, A. Evlyukhin, A. Miroshnichenko, M. Song, E. Nenasheva, and P. Kapitanova, "Anapole meta-atoms: nonradiating electric and magnetic sources," *Phys. Rev. Lett.*, vol. 127, no. 9, p. 096804, 2021.

[41] V. A. Fedotov, A. V. Rogacheva, V. Savinov, D. P. Tsai, and N. I. Zheludev, "Resonant transparency and non-trivial non-radiating excitations in toroidal metamaterials," *Sci. Rep.*, vol. 3, no. 1, p. 2967, 2013.

[42] P. C. Wu, C. Y. Liao, V. Savinov, et al., "Optical anapole metamaterial," *ACS Nano*, vol. 12, no. 2, pp. 1920–1927, 2018.

[43] A. K. Ospanova, I. V. Stenishchev, and A. A. Basharin, "Anapole mode sustaining silicon metamaterials in visible spectral range," *Laser Photonics Rev.*, vol. 12, no. 7, p. 1800005, 2018.

[44] S.-D. Liu, J.-L. Fan, W.-J. Wang, J.-D. Chen, and Z.-H. Chen, "Resonance coupling between molecular excitons and nonradiating anapole modes in silicon nanodisk-J-aggregate heterostructures," *ACS Photonics*, vol. 5, no. 4, pp. 1628–1639, 2018.

[45] R. E. Noskov, I. I. Shishkin, H. Barhom, and P. Ginzburg, "Non-Mie optical resonances in anisotropic biomineral nanoparticles," *Nanoscale*, vol. 10, no. 45, pp. 21031–21040, 2018.

[46] H. Bahrom, A. Goncharenko, L. Fatkhutdinova, et al., "Controllable synthesis of calcium carbonate with different geometry: comprehensive analysis of particle formation, cellular uptake, and biocompatibility," *ACS Sustain. Chem. Eng.*, vol. 7, no. 23, pp. 19142–19156, 2019.

[47] H. Barhom, A. Machnev, R. Noskov, et al., "Biological Kerker effect boosts light collection efficiency in plants," *Nano Lett.*, vol. 19, no. 10, pp. 7062–7071, 2019.

[48] D. Vovchuk, S. Kosulnikov, R. E. Noskov, and P. Ginzburg, "Wire resonator as a broadband Huygens superscatterer," *Phys. Rev. B*, vol. 102, no. 9, 2020, https://doi.org/10.1103/PhysRevB.102.094304.

[49] D. Dobrykh, D. Shakirova, S. Krasikov, et al., "Multipole engineering for enhanced backscattering modulation," *Phys. Rev. B*, vol. 102, no. 19, p. 195129, 2020.

[50] Y. A. Nenasheva, "Ceramic materials for high-quality dielectric resonators of microwave range," *MRS Proc.*, vol. 269, p. 607, 1992.

[51] C. F. Bohren and D. R. Huffman, *Absorption and Scattering of Light by Small Particles*, New York, NY, United States, Wiley, 1998.

[52] L. Wei, Z. Xi, N. Bhattacharya, and H. P. Urbach, "Excitation of the radiationless anapole mode," *Optica*, vol. 3, no. 8, p. 799, 2016.

[53] A. A. Basharin, V. Chuguevsky, N. Volsky, M. Kafesaki, and E. N. Economou, "Extremely high Q-factor metamaterials due to anapole excitation," *Phys. Rev. B*, vol. 95, no. 3, p. 035104, 2017.

[54] K. Baryshnikova, D. Filonov, C. Simovski, et al., "Giant magnetoelectric field separation via anapole-type states in high-index dielectric structures," *Phys. Rev. B*, vol. 98, no. 16, p. 165419, 2018.

[55] E. A. Gurvitz, K. S. Ladutenko, P. A. Dergachev, A. B. Evlyukhin, A. E. Miroshnichenko, and A. S. Shalin, "The high-order toroidal moments and anapole states in all-dielectric photonics," *Laser Photon. Rev.*, vol. 13, no. 5, p. 1800266, 2019.

[56] J. D. Jackson, *Classical Electrodynamics*, 3rd ed. New York, NY, United States, John Wiley & Sons, 1998.

[57] R. Alaee, C. Rockstuhl, and I. Fernandez-Corbaton, "An electromagnetic multipole expansion beyond the long-wavelength approximation," *Opt. Commun.*, vol. 407, pp. 17–21, 2018.

[58] A. B. Evlyukhin, T. Fischer, C. Reinhardt, and B. N. Chichkov, "Optical theorem and multipole scattering of light by arbitrarily shaped nanoparticles," *Phys. Rev. B*, vol. 94, no. 20, p. 205434, 2016.

[59] "Leading global RFID supplier based in New York & Toronto" [Online]. Available at: https://gaorfid.com/.